Anti-fouling Double-Skinned Forward Osmosis Membranes by Constructing Zwitterionic Brushes-decorated MWCNT Ultrathin Film

Xinyu Zhang[†,‡], Ming Xie[§], Zhe Yang[†], Hao-Chen Wu[†], Chuanjie Fang[†], Langming Bai[ǁ], Li-Feng Fang[#], Tomohisa Yoshioka[†], Hideto Matsuyama[†,*]

[†]*Center for Membrane and Film Technology, Department of Chemical Science and Engineering, Kobe University, Kobe 6578501, Japan*

[‡] *College of Chemistry, Chemical Engineering and Materials Science, Soochow University, Suzhou 215123, PR China*

[§] *Department of chemical engineering, University of Bath, BathBA27AY, UK*

[ǁ] *State Key Laboratory of Urban Water Resource and Environment, Harbin Institute of Technology, Harbin 150090, PR China*

[#]*Department of Polymer Science and Engineering,Zhejiang University, Hangzhou310027, PR China*

* Corresponding author.

Email address: matuyama@kobe-u.ac.jp (for Hideto Matsuyama)

Abstract

Pressure retarded osmosis (PRO) process is hindered by severe fouling occurred within porous support of the FO membranes. We designed a novel double-skinned FO membrane containing a polyamide salt-rejecting layer and a zwitterionic brushes-decorated, multi-walled carbon nanotube (MWCNT/PSBMA) foulant-resisting layer on the back side. Our results demonstrated that the coating of MWCNT/PSBMA layer on the porous polyketone (PK) support imparted enhanced hydrophilicity and smaller membrane pore size, thereby providing excellent resistance toward both protein adhesion and bacterial adsorption. We also further evaluated this resultant double-skinned membrane (i.e., TFC-MWCNT/PSBMA) in dynamic PRO fouling experiments, using protein and alginate as model organic foulants. Comparing to the pristine TFC-PK and hydrophobic TFC-MWCNT membranes, the TFC-MWCNT/PSBMA membrane exhibited not only the lowest water flux decline but also the highest water flux recovery after simple physical flushing. These results shed light on fabrication of antifouling PRO membranes for water purification purposes.

Keywords: Forward osmosis; Double-skinned composite membrane; Anti-fouling; zwitterionic brushes; MWCNT

Introduction

With growing global water scarcity, forward osmosis (FO), as a new kind of membrane-based process, has been widely applied in many areas, such as industrial wastewater treatment, seawater desalination, and power generation[1-6]. In an FO process, water permeation is osmotic pressure-driven rather than hydraulic pressure. Therefore, FO process has the advantages of higher water recovery and higher fouling reversibility compared to other pressure-driven membrane processes (e.g. NF or RO)[7-9].

Thin-film composite (TFC) membranes containing a thick porous support and a thin polyamide (PA) selective layer, are the predominant membrane materials of the FO process up to date[10]. Generally, the FO membrane water flux in pressure retarded osmosis (PRO) mode (polyamide layer facing to draw solution) is much higher than the water flux in FO mode (polyamide layer facing to feed solution) because of the suppressed internal concentration polarization (ICP)[11]. However, TFC FO membranes suffer from severer membrane fouling in PRO mode due to the blockage of foulants within the porous support and difficulty in membrane cleaning[12-13]. Therefore, FO process is chosen preferentially to be manipulated under the FO mode for avoiding the membrane fouling, even though the ICP significantly lowers the water flux[12]. Recent studies highlighted the significance of redesigning support structures to maximize the water flux in FO process[14-18]; as such, it is of paramount importance to the development of FO membranes with superior antifouling

properties in PRO mode.

In order to prevent the entry of foulants to the support, constructing an antifouling “barrier” layer on the TFC membrane back side is considered as the most effective approach to alleviate membrane fouling in PRO mode[19-21]. However, technical obstacles to fabricate such a dense layer on the back side are posed by the typical preparation methods of TFC membranes, such as phase separation or interfacial polymerization. So far, extensive studies have attempted to graft soft polymer brushes (e.g. zwitterionic polymer) on the back side to control the fouling in PRO mode[22,23]. These polymer bushes possess strong hydrophilicity and excellent resistance towards foulants caused by their electrostatically induced hydration capacity[24]. However, the large pores with sizes ranging from hundreds of nanometers to a few micrometers on the TFC membrane back side cannot be fully covered with soft polymer brushes with current surface modification approaches. As a result, there is an imperative need to design novel surface modification techniques to specifically block the accumulation of foulants inside the porous support.

Carbon nanotubes (CNTs) have a stable physical and chemical properties, an appropriate mechanical strength and larger length-to-diameter ratio, which have been used in the preparation of the self-supported CNTs filtration membrane[25-28], and CNTs incorporated thin film nanocomposite membranes[29-32]. Better water permeability as well as enhanced anti-fouling capability was usually achieved for these fabricated membranes. Inspired by these studies,

we hypothesize that CNTs can be assembled on the back side of a TFC membrane to alleviate the PRO fouling. The aim of this work is to develop a novel anti-fouling, double-skinned FO membrane containing a polyamide salt-rejecting layer and a zwitterionic brushes-decorated, multi-walled carbon nanotube (MWCNT) foulant-resisting layer. Fouling resistance of the fabricated double-skinned membranes were assessed by static adsorption tests of BSA and *E.coli*. Dynamic fouling experiments further confirmed the effective membrane fouling control in PRO mode by coating a zwitterionic brushes-decorated MWCNT layer on the TFC membrane back side.

Materials and Methods

Materials and Chemicals. Polyketone (PK, Mw=400,000 g mol^{-1}) was obtained from Asahi Kasei Corporation (Japan). Acetone, resorcinol, hexane, and methanol were provided from Wako Pure Chemical Co. (Japan) to fabricate the PK support. 1,3,5-Benzenetricarbonyl trichloride (TMC), 1,3-Phenylenediamine (MPD), Triethylamine (TEA), Sodium dodecyl sulfate (SDS), Hexamethylphosphoric triamide (HMPA), and 10-camphorsulfonic acid (CSA) were ordered from Tokyo Kasei Co. (Japan) to fabricate the polyamide layer. Sodium dodecyl benzene sulfonate (SDBS), bovine serum albumin (BSA), multi-walled carbon nanotube (MWCNT) and alginate were obtained from Sigma-Aldrich Co. (USA). Dopamine hydrochloride (DA), [2-(Methacryloyloxy)ethyl]dimethyl-(3-sulfopropyl)ammonium hydroxide (SBMA),

2-Bromo-2-methylpropionyl bromide (BiBB), N,N-dimethylformamide (DMF), L-ascorbic acid, Tris(2-pyridylmethyl)amine (TPMA), Copper(II) chloride and Tris(hydroxymethyl)aminomethane (Tris) were purchased from J&K Scientific Ltd. (China).

In the protein adsorption test, NaH_2PO_4 and Na_2HPO_4 was used to prepare the phosphate buffer solution (PBS, 0.2 mol/L, pH=7) (Wako, Japan). Albumin-fluorescein isothiocyanate conjugate BSA (FITC-BSA) and Escherichia coli (*E.coli*) (Sigma-Aldrich, USA) were chosen as model protein and bacteria, respectively. Tryptic soy broth (TSB; Becton, Dickinson and Co., USA) was employed as culture medium. SYTO9 (Life Technologies, USA) was chosen to stain the bacteria.

Zwitterionic brushes-decorated MWCNT dispersion preparation. Zwitterionic brushes-decorated MWCNT was prepared by grafting PSBMA brushes on the MWCNT via atom-transfer radical-polymerization (ATRP) methods as shown in **Figure** 1[33]. The grafting yield (GY) was 21%, which was calculated according to the following equation:

$$\mathrm{GY} = \frac{W_b - W_a}{W_a} \times 100\%$$

where W_a is the dried MWCNT weight and W_b is the dried PSBMA modified MWCNT weight. The detailed modification procedures are shown in the Supporting Information. The PSBMA brushes grafted MWCNT is designated as MWCNT/PSBMA and their FT-IR spectra are presented in **Figure** S1. The

successful modification of the PSBMA brushes on MWCNT could be demonstrated by the existence of the two new bands, i.e., sulfonate group at 1035 cm^{-1} and carbonyl group at 1720 cm^{-1}, which are the characteristic peaks of the PSBMA brushes.

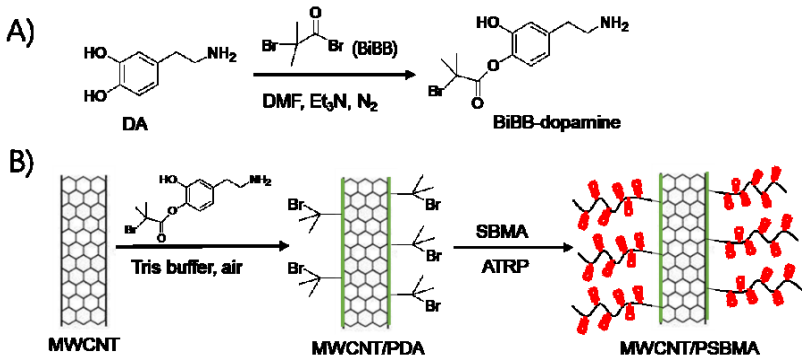

Figure 1. The schematic preparation routes of zwitterionic brushes-decorated MWCNT. (A) Synthetize of BiBB-dopamine. (B) Modification of PSBMA brushes on MWCNT via ATRP (i.e., MWCNT/PSBMA)

The MWCNT/PSBMA dispersion was further prepared according to the previous references[25]. Briefly, 0.1 $g \cdot L^{-1}$ MWCNT/PSBMA powder and 1 $g \cdot L^{-1}$ SDBS were charged into 500 mL fresh water and then put in the ultrasonic cell disruption device at the intensity of 2 kW to sonicate for 5 h. The MWCNT/PSBMA supernatant was subsequently obtained by centrifugal force at 8,000 rpm for 20 min and then was diluted to ~0.08 mg/mL for the following experiments.

Membrane Preparation. The PK support was prepared as follows[34]: briefly, 10 wt% PK power, 58.5 wt% resorcinol and 31.5 wt% water was magnetic stirred in a sealed bottle at 80 °C for 4 h until the mixture became

155 homogeneous. After degassed at 50 °C overnight, this homogenous solution
156 was casted in a height of 300 μm on the neat glass plate and then the whole
157 composite was soaked in a methanol/water (3.5/6.5, w/w) bath for 20 min. The
158 resultant porous PK membrane was sequentially soaked in acetone for 20 min
159 and in hexane for another 20 min, and finally taken out for drying. The
160 illustration of the PK support fabrication step is shown in **Figure** S2 (Supporting
161 Information).

162 **Figure** 2 illustrated the schematic procedure for the preparation of double-
163 skinned FO membrane. Firstly, coating the MWCNT/PSBMA layer on the PK
164 support top side was performed by vacuum-filtered MWCNT/PSBMA
165 dispersion (5 mL) through the PK support[35]. Subsequently, the polyamide layer
166 was interfacial polymerized via the reaction of MPD and TMC on the other side
167 (bottom side) of the PK support according to our previous study[34]. Briefly, the
168 bottom layer of PK support was first exposed to the aqueous MPD solution (1.1
169 wt% TEA, 2.0 wt% MPD, 0.15 wt% SDS, 3.0 wt% HMPA, and 2.3 wt% CSA in
170 water) for 5 min and then followed by wiping the solution from the membrane
171 surface. After that, 0.15 wt% TMC in hexane solution was covered over the
172 bottom layer of PK support for 2 min. The resultant polyamide layer was further
173 deep crosslinked at 90 ˚C for 10 min and then stored in DI water for future usage.
174 These double-skinned membranes based on different second skin layer (e.g.
175 PK layer, MWCNT layer and MWCNT/PSBMA layer) are designated as TFC-
176 PK, TFC-MWCNT and TFC-MWCNT/PSBMA membranes, respectively.

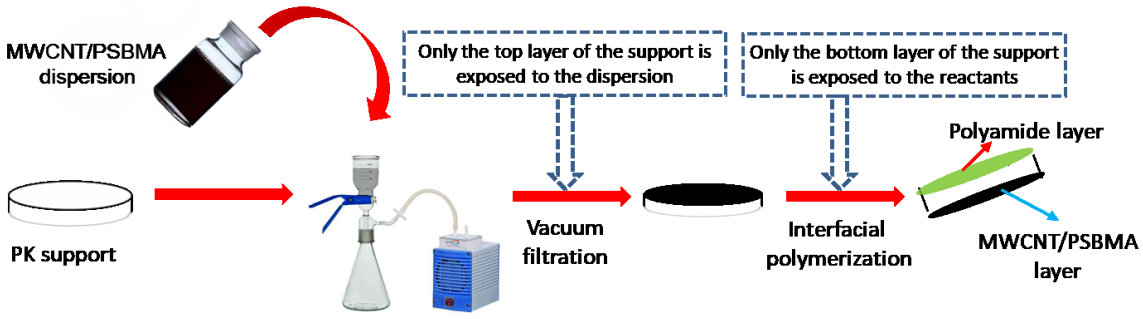

Figure 2. Lab scale fabrication steps for the double-skinned FO membrane.

Membrane Characterizations. Membrane surface morphologies were determined by an atomic force microscopy (AFM, SPA-400, Japan) and a field-emission scanning electron microscope (FE-SEM, JSF-7500, Japan). The membrane surface elemental content was quantified by X-ray photo electron spectroscopy (XPS, JPS-9010MC, JEOL). The surface zeta potential was determined by a SurPASS^{TM} 3 electrokinetic analyzer (Anton Paar, Austria) in a background electrolyte solution (75 mg/L KCl solution). The membrane surface hydrophilicity was characterized by a contact angle meter (DM-300, Japan).

A cross-flow RO setup was employed to evaluate the water permeability (A, $L \cdot m^{-2} \cdot h^{-1} \cdot bar^{-1}$), salt permeability ($B$, $L \cdot m^{-2} \cdot h^{-1}$) and salt rejection rate (R_s, %) of the FO membranes[36]. Structural parameter (S, μm) can be calculated by fitting the A and B values with the FO water flux (J_v, $L \cdot m^{-2} \cdot h^{-1}$)[36]. Detailed information on filtration experiments is described in the Supporting Information.

Static Adhesion Tests. Anti-fouling abilities of the fabricated membranes

were assessed by the static adhesion tests of BSA and *E. coli*[37]. FITC-BSA solution (20 mg/L, pH=7.4) was prepared in a 0.2 mol/L PBS buffer. Membrane samples (0.5 cm x 2 cm) were first soaked into the 2 mL FITC-BSA solution and then shaken at 100 rpm in the dark place for 12 hours. After that, these membrane samples were taken out and then washed twice with fresh PBS buffer. Confocal laser scanning microscopy (CLSM; FV1000D, Japan) was employed to take the fluorescence images.

Membrane adhesion property for bacteria was also evaluated by the static *E*.coli adhesion test as described in reference[37]. First, *E*.coli were precultured in 20 mL of 30 g/L TBS medium overnight at 30 ˚C. And then, 30 g/L TSB medium was used to dilute the *E.coli* suspension 50 times. Next, this *E.coli* suspension was cultivated for another 4 h until its optical density at 450 nm reached to 0.05. Membrane samples (0.5 cm × 2.0 cm) were soaked in the above-prepared *E*.coli suspension (2 mL, pH=7) and shaken at 30 ˚C for 24 h. After that, these membrane samples were washed twice by 0.85 wt% NaCl solution and followed by sequentially soaked in the salty SYTO9 solution (0.85 wt% NaCl) for 20 min, and 2.5 wt% glutaraldehyde solution for 3 min to dye and fix the bacteria, respectively. The resultant membranes were washed and stored in 0.85 wt% NaCl solution until the characterization by using CLSM. The Image J software (National Institutes of Health, MD, USA) was employed to calculate the bacteria coverage.

Membrane Fouling Protocol in PRO mode. A cross-flow FO setup was employed to perform the dynamic fouling experiments in PRO mode (polyamide layer facing to the draw solution) at ambient pressure[19]. In this work, the feed solution at ambient pressure could reflect the PRO operating environment, where no hydraulic pressure is applied in the feed side and the draw side is pressured[38]. All experiments were started with 30 mg/L foulants (BSA or alginate), 0.5 mmol/L $CaCl_2$ and 50 mmol/L NaCl in the feed solution, and an initial water flux of ~30 $L \cdot m^{-2} \cdot h^{-1}$, which was accomplished by controlling the NaCl concentration of draw solution side. The temperature and crossflow velocity of both feed and draw solutions were set at 25 ± 2 °C and 8.5 cm/s, respectively. The fouling experiments were conducted for 10 to 20 hours depending on membranes, until 200 mL of the cumulative permeate volume was attained. Once the fouling run finished, the resultant fouled membrane was physically flushed with fresh water through the both sides of the FO membrane for 30 min at an elevated crossflow velocity of 21 cm/s. To determine the flux recovery, the water flux was obtained again after the cleaning tests using the same but foulant-free feed and draw solutions as in the fouling experiment. To account for the flux drop due to dilution effects, we also carried out the baseline experiments under the same experimental conditions without foulants. The flux decline obtained from fouling experiments has been corrected using the baseline flux profile to account for the dilution effects.

Molecular Dynamic Simulation. To understand the hydrophilicity of different three types of given materials (e.g. CNT, PK, and SBMA), three simulation models contenting these given materials and water molecules were constructed through the Amorphous Cell module with similar atomic numbers, in which the density values were set at 1 g/cm^3 at the outset[39-41]. Detailed information is described in the Supporting Information.

Results and Discussion

Characterizations of the fabricated membranes. The PK support possesses a fully sponge-like structure (**Figure** 3), which can promote the mass transport and provide better mechanical stability during long-term operations. Although visible pores cover on the bottom layer of the PK support (**Figure** 3C), a dense selective polyamide layer consisting of larger “leaf-like” curls is successfully interfacial polymerized on the bottom surface (**Figure** 3F). This may be driven by the special interactions between the MPD solution and the PK matrix[34]. In order to operate the FO membranes in the PRO mode, the top porous surface of the PK support is coated with different second skin layers (e.g. MWCNT and MWCNT/PSBMA layers) via vacuum filtration method. As illustrated in **Figures** 3(G and F) and **Table** S2, the fabricated MWCNT layer has a thickness of 375 nm and a loading density of 322 mg/m^2; for the MWCNT/PSBMA layer, the thickness and loading density are 309 nm and 288 mg/m^2, respectively. As imaged in **Figures** 3D and 3E, compared with the

pristine porous top layer structure (**Figure** 3A), relatively dense and continuous second skin layers are appeared on the top surface of the PK support, evidencing for the successful fabrication. Noting that it is difficult to achieve such a dense coverage of the porous support by using conventional membrane surface modification techniques with soft polymers[42]. The roughness data of these three membranes are shown in **Figure** S3, Supporting Information. MWCNT layer and MWCNT/PSBMA layer are smoother than the PK support surface.

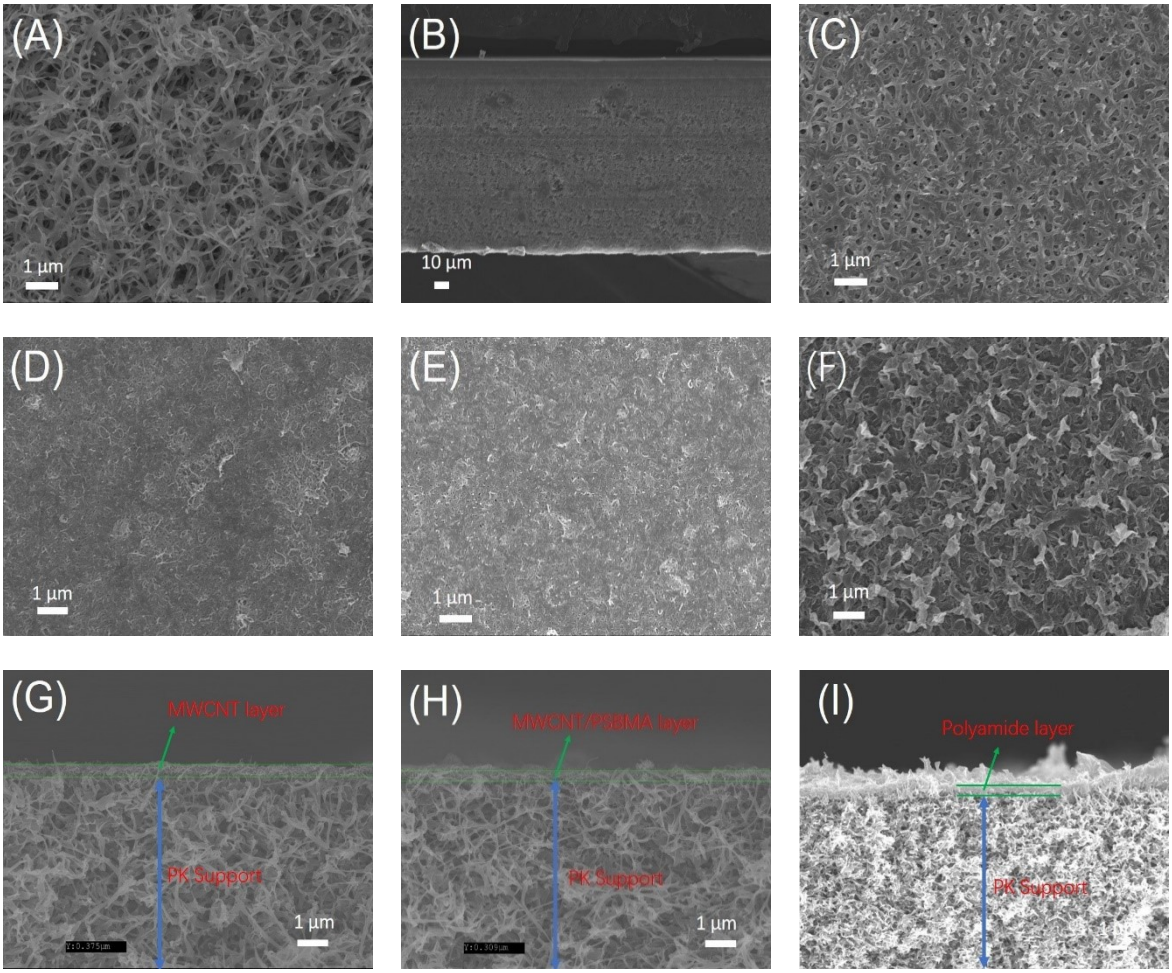

Figure 3. SEM micrographs of the (A) top surface, (B) cross-section and (c) bottom surface of the PK support surface; Morphologies of the (D) MWCNT surface and (E)

MWCNT/PSBMA surface after vacuum suction of carbon nanotube dispersion onto the top of PK support; Morphology of the (F) polyamide layer after interfacial polymerization on the bottom of PK support. Cross-sections of the (G) MWCNT layer, (H) MWCNT/PSBMA layer and (I) polyamide layer.

At the same time, the mean pore sizes of the three different supports are estimated based on the PEO rejection coefficient and the corresponding pore size distributions are plotted as the probability density function[17]. Details of PEO rejection experiment and determination of pore size distribution are described in the Supporting Information. As shown in **Figure** 4A and **Table** S1, the top surface of PK support has the largest mean pore size (54.6 nm) and MWCO value (369 KDa). After coating the carbon nanotube layer on the PK support, the mean pore sizes are decreased to 17.8 nm (corresponding to MWCO of 131 KDa) and 13.2 nm (corresponding to MWCO of 121 KDa) for MWCNT layer and MWCNT/PSBMA layer, respectively. These results agreed well with the surface morphology change as shown in **Figure** 3. Compared to the MWCNT layer, the smaller mean pore size of the MWCNT/PSBMA layer may be ascribed to the swelling chain conformation of PSBMA brushes in the water[24,43]. In here, the degree of PSBMA swelling (DS) is ~15.5%, which is defined as: DS = W_w/W_d, where W_w and W_d are the wetted and dried weight of PSBMA modified MWCNT, respectively. Furthermore, the pristine PK support exhibits the lowest rejection towards BSA (0%) and alginate (44.4%); on the contrary, the MWCNT/PSBMA layer has the highest rejection towards BSA (13.2%) and alginate (71.3%) as shown in **Table** S2. As a general rule, the rejection property of the asymmetric porous membrane is mainly dominated by the top layer.

Accordingly, our results demonstrate the successful fabrication of zwitterionic brushes-decorated MWCNT layer on PK support.

The membrane surface chemistries of different second skin layers can be successfully verified by XPS technique. XPS wide scan spectra are shown in **Figure** S4. As shown in **Figure** 4B, the PK support consists of “C” (~78.5%) and “O” (~24.5%), which matches well with the elemental composition of PK molecule. After the MWCNT layer coating on the PK support, “C” (~96.9%) becomes the primary element and “O” (~3.1%) is detected in a very low composition concentration. This noticeable change indicates the complete covering of MWCNT layer on the PK support. In the case of TFC-MWCNT/PSBMA membrane, more than the primary element of “C” (~84.4%) and “N” (~12.2%), the presence of “S” (~1.4%) and “N” (~2%) confirms the successful coating of MWCNT/PSBMA layer on the PK support.

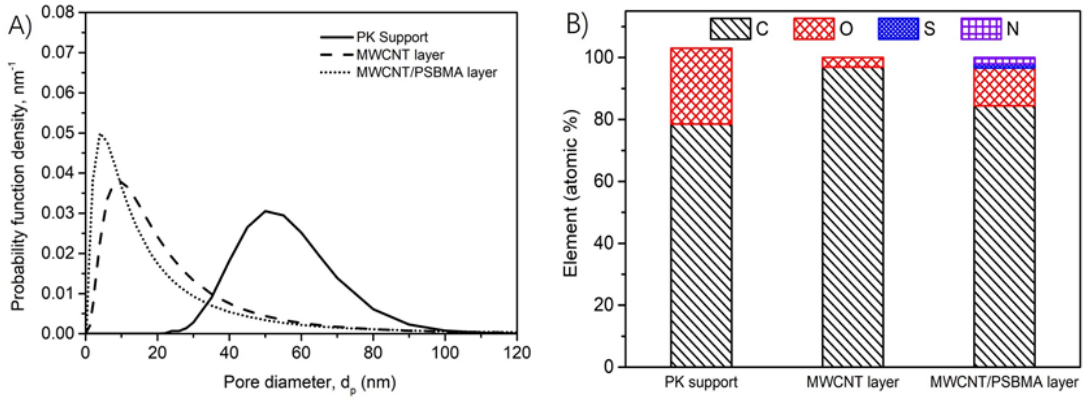

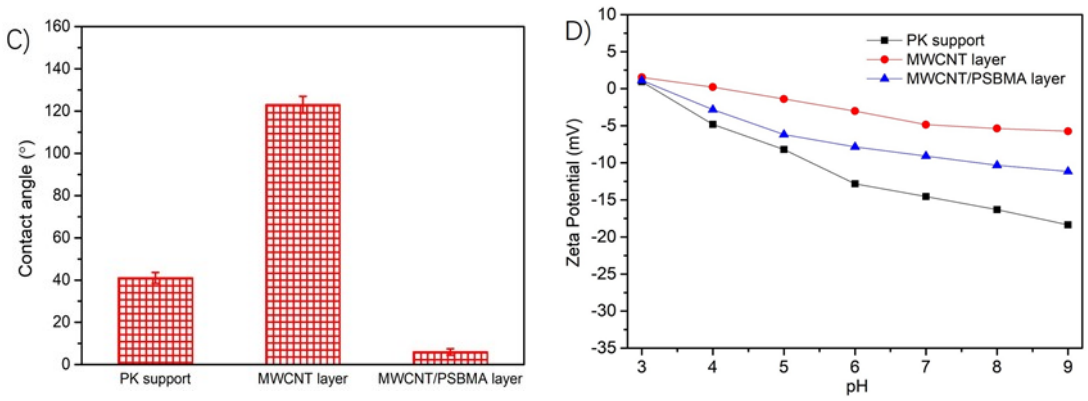

Figure 4. Key membrane characteristics: (A) surface pore size distributions, (B) XPS spectroscopy, (C) water contact angles, and (D) zeta potentials as a function of pH of the PK support, MWCNT layer and MWCNT/PSBMA layer of the double-skin layer membrane.

Water contact angle (CA) measurement was employed to assess the surface hydrophilicity. As illustrated in **Figure** 4C, the PK support surface exhibits a CA of ~41º, which is consistent with previously published data[44]. On the other side, the CA of MWCNT layer is significantly increased to ~123º, indicating its hydrophobic nature due to the aromatic rings of carbon nanotube. For the zwitterionic PSBMA brushes decorated MWCNT layer, a definite reduction of CA to ~6º is observed, which evidences a hydrophilic surface due to the grafted PSBMA brushes and may significantly enhance its fouling resistance.

Membrane surface charges were characterized by zeta potential measurements and the results are exhibited in **Figure** 4D. For the experimental pH range (e.g., pH 3-9), the PK support zeta potential is slightly positive (e.g., 1 mV at pH 3) at the beginning and then increasingly negative with the growing pH due to the preferential anion adsorption to the weaker hydrated PK surface. This result reflects the characteristic charge curve of non-ionic surface, such as

polysulfone membrane[45,46]. After coating the MWCNT layer on the PK support, the zeta potential becomes least negative due to the presence of the most hydrophobic MWCNT shielding on the PK support, which reduces the anion adsorption to a great extent. Compared with the MWCNT layer, the MWCNT/PSBMA layer exhibits slightly more negative, being consistent with the previous studies[24,33,47]. Guo et al.[48] explained that the slight negative charge of PSBMA brushes can be ascribed to its overall acidic characteristic in solution, since the pK_a value of sulfonate groups is 2 and pK_b value of quaternary ammonium groups is 5.

Membrane Intrinsic Transport Properties. As summarized in **Table** 1, the *A* values of the double-skinned membranes (1.87 and 1.93 $L \cdot m^{-2} \cdot h^{-1} \cdot bar^{-1}$ for TFC-MWCNT and TFC-MWCNT/PSBMA membranes, respectively) remain almost the same as that of TFC-PK membrane (2.0 $L \cdot m^{-2} \cdot h^{-1} \cdot bar^{-1}$); while the *B* values increases lightly from 0.38 $L \cdot m^{-2} \cdot h^{-1}$ for TFC-PK membrane to 0.59 and 0.51 $L \cdot m^{-2} \cdot h^{-1}$ for TFC-MWCNT and TFC-MWCNT/PSBMA membranes, respectively. It is because A and B values are the intrinsic parameters relevant only to the polyamide layer. The *S* values, relevant only to the supporting layer, increase slightly but not statistically significant after deposition of carbon nanotube layer on the top of PK support (263 μm vs 330 μm vs 306 μm for the TFC-PK, TFC-MWCNT and TFC-MWCNT/PSBMA membranes, respectively). These results demonstrate that the nanoscale thicknesses of carbon tube

353 layers have no effect on the transport properties of the double-skinned
354 membranes[49].

355

356 **Table 1.** Intrinsic properties, structural parameters and salt rejections of the double-
357 skinned membranes (Detailed testing methods are shown in Supporting Information)
358

Membrane code	A (L·m^{-2}·h^{-1}·bar^{-1})	B （L·m^{-2}·h^{-1}）	S (μm)	R_s (%)
TFC-PK	2.00±0.10	0.38±0.10	263±11	97.7±0.2
TFC-MWCNT	1.87±0.21	0.59±0.08	330±7	96.1±0.1
TFC-MWCNT/PSBMA	1.93±0.12	0.51±0.10	306±10	96.8±0.1

359

360 **Interaction energy between membrane materials and water molecules.**
361 The notably enhanced hydrophilicity of the MWCNT/PSBMA surface suggests
362 that the anti-fouling properties may be improved because of the PSBMA
363 brushes grafting. In order to understand the hydrophilicity of three different
364 types of given materials (e.g. PK, MWCNT and PSBMA), molecular dynamics
365 simulation technique was employed to explore the interactions. During the
366 simulation process, the interaction between the polymer chain and water
367 molecules was recorded and analyzed to further compare the hydration
368 capacities of these three types of membrane materials.

369 **Figure** 5 presents the interaction energy and intermolecular H-bonds
370 between membrane materials and water molecules. As shown in **Figures** 5B
371 and 5C, interaction energy between MWCNT and water molecules displays the
372 largest value of −89.5 kcal/mol, with almost zero H-bonds. This highest energy
373 can be ascribed to the hydrophobicity of MWCNT, demonstrating that the

attachment of organic foulants on its surface could occur easily to minimize the interfacial energy[50]. For PK polymer, the interaction energy is decreased to -249.2 kcal/mol, exhibiting H-bonds with a middle number of 24.8. In contrast, the zwitterionic PSBMA polymer shows the lowest interaction energy value, −886.8 kcal/mol, representing 71.9% reduction in interaction energy compared to the PK polymer. Also, the H-bond number is the highest value of 43. These results are due to its special interactions with water. In addition to the hydrogen bonding between water molecules and PK polymer, zwitterionic PSBMA polymers can strongly trap water molecules via the electrostatic force to form a more tighter hydration layer (**Figure** 5A)[23,24,51]. This hydration layer would prevent organic foulants from close contact with the modified surface due to no significant thermodynamic advantage[52].

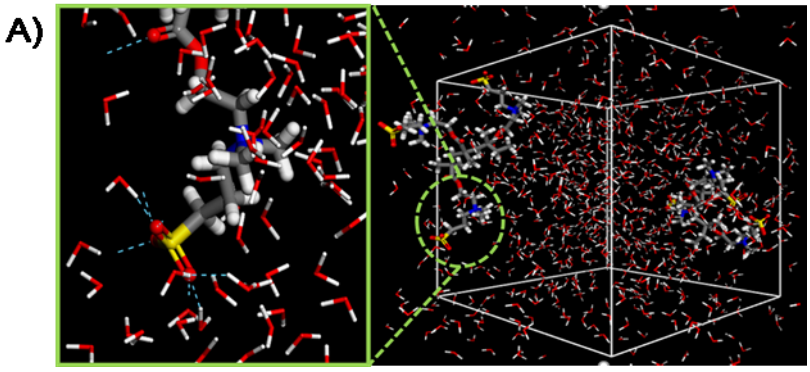

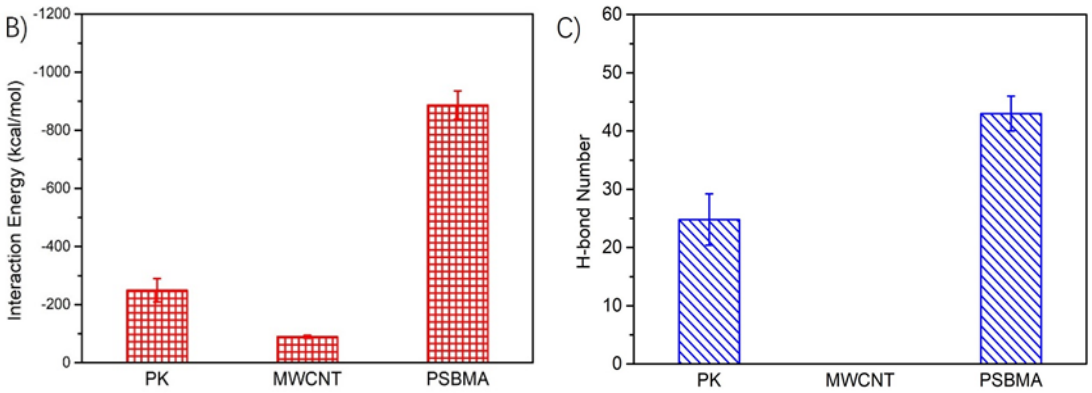

Figure 5. Molecular dynamics simulation. (A) H-bonds network between PSBMA and water molecules; The atom colors are chosen as follows: C, gray; N, blue; O, red; S, yellow; H, white. (B) Interaction energy between PK, MWCNT, PSBMA and water molecules, respectively; (C) Intermolecular H-bond number between PK, MWCNT, PSBMA and water molecules, respectively.

Adsorption Propensity of Proteins and Bacteria. Anti-fouling properties of the double-skinned membranes were evaluated by its resistance against protein and bacteria adsorption. As the typical protein and bacteria, BSA and *E*. coli, are used as model organic foulants, respectively. Their accumulation on the membrane surface not only compromises the water flux, but also forms a conditioning film, which could provide carbon and nitrogen sources for the microbial colonization[53-55]. Therefore, protein fouling resistance is considered as one of the important factors to investigate the anti-fouling properties of double-skinned membranes.

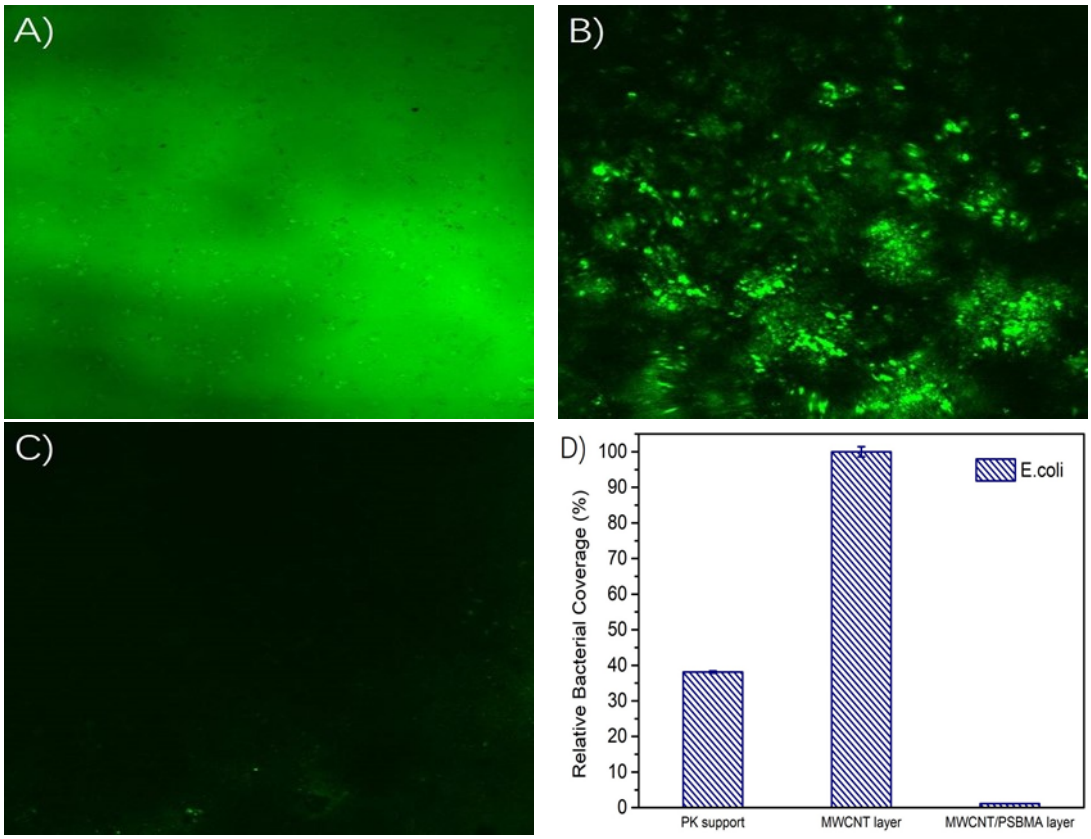

Figure 6. CLSM images of (A) PK support, (B) MWCNT layer, and (C) MWCNT/PSBMA layer after protein adhesion tests using FITC-BSA in PBS. TFC-PK, TFC-MWCNT, and TFC-MWCNT/PSBMA after 12 h exposure to FITC-BSA in 0.2 M PBS at pH=7. (D) Relative adhesion of E. coli on the PK support, MWCNT layer and MWCNT/PSBMA layer of FO membranes after 24 h contact time, normalized to the result of the MWCNT surface.

Surface fluorescence intensities were adopted to evaluate the protein adsorption after exposure to fluorescein-labeled BSA (FITC-BSA). Fluorescence images of the PK support, MWCNT layer and MWCNT/PSBMA layer of the double-skinned membranes are showed in **Figure** 6. The fluorescence intensities can directly quantify the BSA adsorption degrees on membrane surfaces. Despite having a relatively hydrophilic PK surface, the TFC-PK membrane still has a brightest fluorescence image (**Figure** 6A). This may be because the protein not only on the surface but also underneath the surface can be determined by the fluorescence[23], especially for the porous PK

surface. **Figure** 6B illustrates that the MWCNT layer has a slightly weaker fluorescence intensity due to the deceased surface pore size, while the MWCNT/PSBMA layer exhibits virtually no fluorescence (**Figure** 6C). It can conclude that the MWCNT/PSBMA layer possesses the excellent anti-fouling property toward protein. This difference between the MWCNT layer and MWCNT/PSBMA layer can be ascribed to the fact that the benzene rings of the former could attract proteins while the latter has unique interactions with water and inhibits the protein adsorption.

Bacteria adsorption tests were also conducted with *E*. coli to inspect the anti-microbial abilities of the fabricated membranes. As illustrated in **Figure** 6D, the MWCNT layer has the highest bacteria attachment. After coating with the zwitterionic brushes-decorated MWCNT layer, the TFC-MWCNT/PSBMA membrane exhibits a higher anti-adhesive property toward bacteria, with bacterial coverage reduction of 37% compared to the TFC-PK membrane.

Dynamic Fouling Behavior in PRO mode. Anti-fouling properties of the fabricated membranes were assessed by the dynamic BSA and alginate fouling experiments, when they were tested in PRO mode (membrane polyamide layer facing to the draw solution). Immediately after fouling, physical flushing with higher crossflow rate of 21 cm/s was used to clean the fouled membranes for 30 min. **Figure** 7 shows the declined flux induced by organic fouling and the recovered flux after physical cleaning.

The TFC-PK membrane, with a porous back side surface, exhibits the most severe flux decline to 33% of its initial water flux owing to the significant BSA fouling (**Figures** 7A and 7C). The foulant blockage within the porous support of the TFC-PK membrane significantly deteriorates the membrane filtration capacity. By contrast, the TFC-MWCNT/PSBMA membrane whose back surface sealed with a hydrophilic MWCNT/PSBMA layer, exhibits an improved flux stability with an 85% retention of the initial water flux. This result demonstrates the excellent antifouling performance towards BSA foulant of MWCNT/PSBMA surface, which is consistent to its decreased surface pore sizes and enhanced hydrophilic properties. Besides, the TFC-MWCNT membrane has a weaker anti-fouling property with a reduction to 60% of its initial flux. This is because its most hydrophobic MWCNT surface are easy subjected to strong BSA foulant adhesion, which matches well with the results in the static fouling experiments (Section **3.4**).

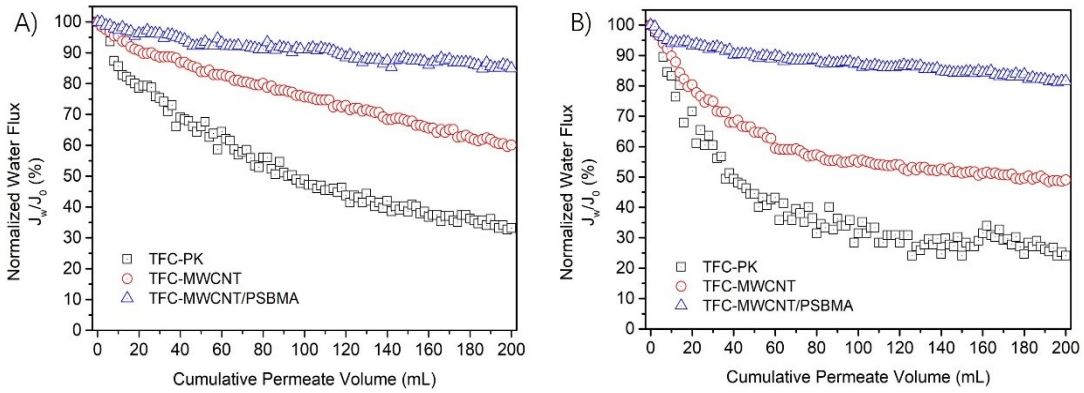

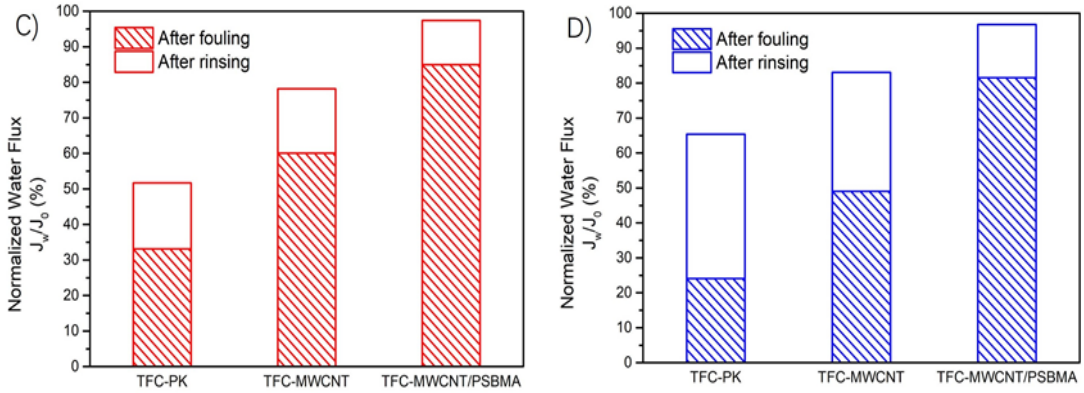

Figure 7. Water flux decline curves for TFC-PK, TFC-MWCNT, and TFC-MWCNT/PSBMA membranes obtained from (A) BSA and (B) alginate fouling experiments. Feed solution was prepared by adding 30 mg/L foulants and 0.5 mmol/L $CaCl_2$ to 50 mmol/L NaCl. Summarized organic fouling results of (C) BSA and (D) alginate fouling experiments with TFC-PK, TFC-MWCNT, and TFC-MWCNT/PSBMA membranes. Blank columns mean the percentage of flux recovery after physical cleaning.

Compared with BSA fouling, alginate fouling causes more flux decline (**Figure** 7B), especially for the TFC-PK and TFC-MWCNT membranes under the same tested conditions. As an end of membrane fouling, the water fluxes of the TFC-PK and TFC-MWCNT membranes decrease to 24% and 49% of the initial water flux, respectively. Ca^{2+} ions (0.5 mmol/L) in the feed solution is known to aggravate alginate fouling by acting as “bridges” between alginate molecules, which leads to form a cross-linked gel-like alginate on the PK and MWCNT surfaces and thus causes a significant decrease of water flux[56,57]. By comparison, the alginate fouling of the TFC-MWCNT/PSBMA membrane is still the least severe with a highest flux retention up to 82% of its initial value, again demonstrating the outstanding anti-fouling abilities of the hydrophilic MWCNT/PSBMA surface.

The above-mentioned filtration performance can be further reinforced by

an apparent discrepancy in the water flux recovery efficiencies for these three membranes as shown in **Figures** 7C and 7D; the flux recovery of the fouled membranes follows the order of TFC-PK membrane<TFC-MWCNT membrane<TFC-MWCNT/PSBMA membrane. For the TFC-PK membrane, the foulants blocked into the porous PK support, cannot be eliminated by the shear force of physical cleaning, which leads to severe irreversible fouling. On the other hand, the MWCNT/PSBMA layer created on the PK support could defense against the intruding of agglomerated foulants (e.g. alginate gels) into the pores of PK support, which makes the foulants only possibly deposit on the surface. The shear force of physical cleaning could easily flush these deposited foulants away from the membrane surface, and thus the water flux can be satisfactorily recovered. These anti-fouling mechanisms can be further demonstrated by the SEM images of fouled TFC-MWCNT/PSBMA membrane. As shown in **Figure** 8A, the agglomerated organic foulants (e.g. alginate gels) scatter randomly on the MWCNT/PSBMA surface rather than in the inner PK support (**Figure** 8B). The cleaned surface is also analyzed and exhibits almost no fouling surface coverage (**Figure** 8C). Taken together, the overall antifouling performance of the TFC-MWCNT/PSBMA membrane is better than the other two membranes when operated in PRO mode, highlighting a versatile approach to design antifouling FO membranes.

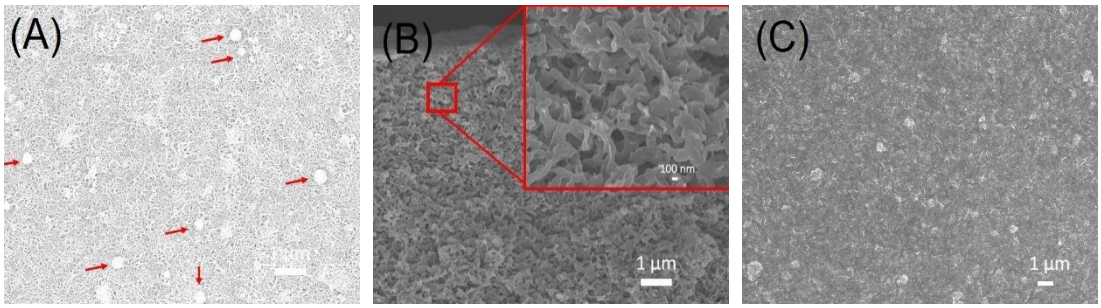

Figure 8. SEM images of MWCNT/PSBMA surface and cross-section (near the MWCNT/PSBMA layer) of (A, B) fouled and (C) cleaned TFC-MWCNT/PSBMA membrane. Note: The red arrow in Figure 8A means the alginate gels. The inset in Figure 8B is the cross-section image of PK support at 100 nm scale.

Conclusion

In this work, we have successfully designed an anti-fouling double-skinned FO membrane by constructing zwitterionic brushes-decorated MWCNT layer on the PK support for improving the organic fouling resistance under PRO mode. Surface characterization revealed that the introduction of MWCNT/PSBMA layer could significantly alter the surface morphologies of the PK support, such as enhanced hydrophilicity, reduced surface roughness and narrowed surface pored size. Computational methods provided insights into the excellent hydrophilic nature of zwitterionic PSBMA brushes, and thus the MWCNT/PSBMA layer surface exhibited the best anti-protein adsorption and anti-bacterial adhesion properties. In dynamic PRO fouling tests, coating a MWCNT/PSBMA layer on the PK support achieved the least negative effects on water flux and the highest recovered water flux in comparison of the pristine TFC-PK and hydrophobic TFC-MWCNT membranes.

Acknowledgments

This work was supported by Kurita Water and Environment Foundation (No. 16A073) to D.S., and Creation of Innovation Centers for Advanced Interdisciplinary Research Areas (Innovative Bioproduction, Kobe) from the Ministry of Education, Culture, Sports, Science and Technology of Japan.

Appendix A. Supporting information

Supplementary data associated with this article can be found in the online version at ……

Reference

[1] McGinnis, R. L.; Elimelech, M. Global challenges in energy and water supply: The promise of engineered osmosis, Environ. Sci. Technol. **2008**, 42, 8625-8629.

[2] Coday, B. D.; Xu, P.; Beaudry, E. G.; Herron, J.; Lampi, K.; Hancock, N. T.; Cath, T. Y. The sweet spot of forward osmosis: Treatment of produced water, drilling wastewater, and other complex and difficult liquid streams. Desalination **2014**, 333, 23-35.

[3] Lutchmiah, K.; Verliefde, A. R. D.; Roest, K.; Rietveld, L. C.; Cornelissen, E. R. Forward osmosis for application in wastewater treatment: A review. Water Res. **2014**, 58, 179-197.

[4] Akther, N.; Sodiq, A.; Giwa, A.; Daer, S.; Arafat, H. A.; Hasan, S. W. Recent advancements in forwards osmosis desalination: A review. Chem. Eng. J. **2015**, 281, 502-522.

[5] Chekli, L.; Phuntsho, S.; Kim, J. E.; Kim J.; Choi, J. Y.; Choi, J. S.; Kim, S.; Kim, J. H.; Hong, S.; Sohn, J.; Shon, H. K. A comprehensive review of hybrid forward osmosis systems: Performance, applications and future prospects. J. Membr. Sci.**2016**, 497, 430-449.

[6] Linares, R. V.; Li, Z.; Yangali-Quintanilla, V.; Ghaffour, N.; Amy, G.; Leiknes, T.; Vrouwenvelder, J. S. Life cycle cost of a hybrid forward osmosis-low pressure reverse osmosis system for seawater desalination and wastewater recovery. Water Res. **2016**, 88,

225-234.

[7] Lee, S.; Boo, C.; Elimelech, M.; Hong, S. Comparison of fouling behavior in forward osmosis (FO) and reverse osmosis (RO). J. Membr. Sci. **2010**, 365, 34-39.

[8] Mi, B.; Elimelech, M. Organic fouling of forward osmosis membranes: fouling reversibility and cleaning without chemical reagents. J. Membr. Sci. **2010**, 348, 337-345.

[9] Kwan, S. E.; Bar-Zeev, E.; Elimelech, M. Biofouling in forward osmosis and reverse osmosis: measurements and mechanisms. J. Membr. Sci. **2015**, 493, 703-708.

[10] Werber, J. R.; Osuji, C. O.; Elimelech, M. Materials for next generation desalination and water purification membranes. Nature Reviews Materials **2016**, 1, 16018.

[11] Zhao, S.; Zou, L.; Tang, C. Y.; Mulcahy, D. Recent developments in forward osmosis: Opportunities and challenges. J. Membr. Sci.**2012**, 396, 1-21.

[12] Tang, C. Y.; She, Q.; Lay, W. C. L.; Wang. R.; Fane, A. G. Coupled effects of internal concentration polarization and fouling on flux behavior of forward osmosis membranes during humic acid filtration. J. Membr. Sci.**2010**, 354, 123-133.

[13] Zhao, S.; Zou, L.; Mulcahy, D. Effects of membrane orientation on process performance in forward osmosis applications. J. Membr. Sci.**2011**, 382, 308-315.

[14] Yip, N. Y. Y.; Tiraferri, A.; Phillip, W. A.; Schiffman, J. D.; Elimelech, M. High performance thin-film composite forward osmosis membrane. Environ. Sci. Technol. **2010**, 44, 3812-3818.

[15] Wang, R.; Shi, L.; Tang, C. Y.; Chou, S.; Qiu, C.; Fane, A. G. Characterization of novel forward osmosis hollow fiber membranes. J. Membr. Sci.**2010**, 355, 158-167.

[16] Wei, J.; Qiu, C.; Tang, C. Y.; Wang, R.; Fane. A. G. Synthesis and characterization of flat-sheet thin film composite forward osmosis membranes. J. Membr. Sci.**2011**, 372, 292-302.

[17] Zhang, X. Y.; Tian, J. Y.; Ren, Z. J.; Shi, W. X.; Zhang, Z. B.; Xu, Y. B.; Gao. S. S. Cui, F. Y. High performance thin-film composite (TFC) forward osmosis (FO) membrane fabricated on novel hydrophilic disulfonated poly(arylene ether sulfone) multiblock copolymer/polysulfone substrate. J. Membr. Sci. **2016**, 520, 529-539.

[18] Emadzadeh, D.; Lau, W. J.; Matsuura, T.; Rahbari-Sisakht, M.; Ismail, A. F. A novel thin film composite forward osmosis membrane prepared from PSf-TiO_2 nanocomposite substrate for water desalination. Chem. Eng. J. **2014**, 237, 70-80.

[19] Hu, M.; Zheng, S. X.; Mi, B. X. Organic fouling of graphene oxide membranes and its implications for membrane fouling control in engineered osmosis. Environ. Sci. Technol.

2016, 50, 685−693.
[20] Qi, S. R.; Qiu, C. Q.; Zhao, Y.; Tang, C. Y. Y. Double-skinned forward osmosis membranes based on layer-by-layer assembly-FO performance and fouling behavior. J. Membr. Sci. **2012**, 405, 20−29.
[21] Li, X.; Cai, T.; Chung, T. S. Anti-fouling behavior of hyperbranched polyglycerol-grafted poly(ether sulfone) hollow fiber membranes for osmotic power generation. Environ. Sci. Technol. **2014**, 48, 9898-9907.
[22] Zhao, D. L.; Qiu, G. L.; Li, X.; Wan, C. F.; Lu, K. J.; Chung, T. S. Zwitterions coated hollow fiber membranes with enhanced antifouling properties for osmotic power generation from municipal wastewater. Water Res. **2016**, 104, 389-396.
[23] Le, N. L.; Quilitzsch, M.; Cheng, H.; Hong, P. Y.; Ulbricht, M.; Nunes, S. P.; Chung, T. S. Hollow fiber membrane lumen modified by polyzwitterionic grafting. J. Membr. Sci.**2017**, 522, 1-11.
[24] Liu, C. H.; Lee, J.; Ma, J.; Elimelech, M. Antifouling thin-film composite membranes by controlled architecture of zwitterionic polymer brush layer. Environ. Sci. Technol. **2017**, 51, 2161−2169.
[25] Gao, S. J.; Zhu, Y. Z.; Zhang, F.; Jin, J. Superwetting polymer-decorated SWCNT composite ultrathin films for ultrafast separation of oil-in-water nanoemulsions. J. Mater. Chem. A. **2015**, 3, 2895-2902.
[26] An, Y. P.; Yang, J.; Yang, H. C.; Wu, M. B.; Xu, Z. K. Janus membranes with charges carbon nanotube coatings for deemulsification and separation of oil-in-water emulsions. ACS Appl. Mater. Interfaces **2018**, 10, 9832−9840.
[27] Fan, X. F.; Liu, Y. M.; Quan, X.; Chen, S. Highly permeable thin-film composite forward osmosis membrane based on carbon nanotube hollow fiber scaffold with electrically enhanced fouling resistance. Environ. Sci. Technol. **2018**, 52, 3, 1444-1452.
[28] Jia, Y. X.; Li, H. L.; Wang, M.; Wu, L. Y.; Hu, Y. D. Carbon nanotube: Possible candidate for forward osmosis. Sep. Purif. Technol. **2010**, 24, 55-60.
[29] Ma, X. H.; Guo, H.; Yang, Z.; Yao, Z. K.; Qing, W. H.; Chen, Y. L.; Xu, Z. L.; Tang, C. Y. Y. Carbon nanotubes enhance permeability of ultrathin polyamide rejection layers. J. Membr. Sci. **2019**, 570-571, 139-145.
[30] Morales-Torres, S.; Esteves, C. M. P.; Figueiredo, J. L.; Siva, A. M. T. Thin-film composite forward osmosis membranes based on polysulfone supports blended with nanostructured carbon materials. J. Membr. Sci. **2016**, 520, 326-336.

[31] Zhou, Z. Y.; Hu, Y. X.; Boo, C. H.; Liu, Z. Y.; Li, J. Q.; Deng, L. Y.; An, X. C. High-performance thin-film composite membrane with an ultrathin spray-coated carbon nanotube interlayer. Environ. Sci. Technol. Lett. **2018**, 5, 243−248.

[32] Li, D.; Yan, Y. S.; Wang, H. T. Recent advances in polymer and polymer composite membranes for reverse and forward osmosis processes. Prog. Polym. Sci. **2016**, 61, 104-155.

[33] Zhang, X. Y.; Tian, J. Y.; Gao, S. S.; Shi, W. X.; Zhang, Z. B.; Cui, F. Y.; Zhang, S. M.; Guo, S. N.; Yang, X. N.; Xie, H.; Liu, D. M. Surface functionalization of TFC FO membranes with zwitterionic polymers: Improvement of antifouling and salt-responsive cleaning properties. J. Membr. Sci. **2017**, 544, 368-377.

[34] Fang, L. F.; Cheng, L.; Jeon, S.; Wang, S. Y.; Takahashi, T.; Matsuyama, H. Effect of the supporting layer structures on antifouling properties of forward osmosis membranes in AL-DS mode. J. Membr. Sci. **2018**, 552, 265-273.

[35] Shi, Z.; Chen, X. J.; Wang, X. W.; Zhang, T.; Jin, J. Fabrication of superstrong ultrathin free-standing single-walled carbon nanotube films via a wet process. Adv. Funct. Mater. **2011**, 21, 4358–4363.

[36] Zhang, X. Y.; Tian, J. Y.; Gao, S. S.; Zhang, Z. B.; Cui, F. Y.; Tang, C. Y. In situ surface modification of thin film composite forward osmosis membranes with sulfonated poly(arylene ether sulfone) for anti-fouling in emulsified oil/water separation. J. Membr. Sci. **2017**, 527, 26-34.

[37] Yang, Z.; Saeki, D.; Matsuyama, H. Zwitterionic polymer modification of polyamide reverse-osmosis membranes via surface amination and atom transfer radical polymerization for anti-biofouling. J. Membr. Sci. **2018**, 550, 332-339.

[38] Yip, N. Y.; Elimelech, M. Influence of natural organic matter fouling and osmotic backwash on pressure retarded osmosis energy production from natural salinity gradients. Environ. Sci. Technol. **2013**, 47, 12607−12616.

[39] Sun, H. COMPASS: An ab Initio Force-Field Optimized for Condensed-Phase Applications-Overview with Details on Alkane and Benzene Compounds. J. Phys. Chem. B, **1998**, 102, 7338-7364.

[40] Sun, H.; Ren, P.; Fried, J. R. The COMPASS force field: parameterization and validation for phosphazenes. Comput. Theor. Polm. S. **1998**, 8, 229-246.

[41] Sun, H.; Jin, Z.; Yang, C. W.; Akkermans, R. L. C.; Robertson, S. H.; Spenley, N. A.; Miller, S.; Todd, S. M. COMPASS II: extended coverage for polymer and drug-like molecule

644 databases, J.Mol. Model. **2016**, 22, 47.
645 [42] Ong, C. S.; Al-anzi, B.; Lau, W. J.; Goh, P. S.; Lai, G. S.; Ismail, A. F.; Ong, Y. S. Anti-
646 fouling double-skinned forward osmosis membrane with zwitterionic brush for oily
647 wastewater treatment. Scientific Reports **2017**, 7, 6904.
648 [43] Haraguchi, K.; Ning, J. Y.; Li, G. Swelling/deswelling behavior of zwitterionic
649 nanocomposite gels consisting of sulfobetaine polymer-clay networks. Eur. Polym. J. **2015**,
650 68, 630-640.
651 [44] Zhang, L.; Cheng, L.; Wu, H. C.; Yoshioka, T.; Matsuyama, H. One-step fabrication of
652 robust and anti-oil-fouling aliphatic polyketone composite membranes for sustainable and
653 efficient filtration of oil-in-water emulsions. J. Mater. Chem. A, **2018**, 6,24641-24650.
654 [45] Mőckel, D.; Staude, E.; Dal-Cin, M.; Darcovich, K.; Guiver, M. Tangential flow
655 streaming potential measurements: Hydrodynamic cell characterization and zeta potentials
656 of carboxylatedpolysulfone membranes. J. Membr. Sci.**1998**, 145, 211-222.
657 [46] Ariza, M. J.; Benavente, J. Streaming potential along the surface of polysulfone
658 membranes: A comparative study between two different experimental systems and
659 determination of electrokinetic and adsorption parameters. J. Membr. Sci.**2001**, 190, 119-
660 132.
661 [47] Jiang, S.; Cao, Z. Ultralow-fouling, functionalizable, and hydrolyzable zwitterionic
662 materials and their derivatives for biological applications. Adv. Mater. **2010**, 22 (9), 920−32.
663 [48] Guo, S. S.; Jańczewski, D.; Zhu, X. Y.; Quintana, R.; He, T.; Neoh, K. G. Surface
664 charge control for zwitterionic polymer brushes: Tailoring surface properties to antifouling
665 applications. J. Colloid Interf. Sci. **2015**, 452, 43-53.
666 [49] Zhang, X.; Shen, L.; Guan, C. Y.; Liu, C. X.; Lang, W. Z.; Wang, Y. Construction of
667 SO_2@MWNTs incorporated PVDF substrate for reducing internal concentration
668 polarization in forward osmosis. J. Membr. Sci. **2018**, 564, 328-341.
669 [50] Krishnan, S.; Weinman, C. J.; Ober, C. K. Advances in polymers for anti-biofouling
670 surfaces. J. Mater. Chem., **2008**,18, 3405-3413
671 [51] Laughlin, R. G. Fundamentals of the zwitterionic hydrophilic group. Langmuir **1991**, 7,
672 842−847.
673 [52] He, M.; Gao, K.; Zhou, L.; Jiao, Z.; Wu, M.; Cao, J.; You, X.; Cai, Z.; Su, Y.; Jiang, Z.
674 Zwitterionic materials for antifouling membrane surface construction. Acta Biomater. **2016**,
675 40, 142−152.
676 [53] Banerjee, I.; Pangule, R. C.; Kane, R. S. Antifouling coatings: Recent developments

677 in the design of surfaces that prevent fouling by proteins, bacteria, and marine organisms.
678 Adv. Mater. **2011**, 23, 690–718.
679 [54] Guo, W.; Ngo, H.H.; Li, J. A mini-review on membrane fouling. Bioresour. Technol.
680 **2012**, 122, 27−34.
681 [55] Roosjen, A.; van der Mei, H. C.; Busscher, H. J.; Norde, W. Microbial adhesion to
682 poly(ethylene oxide) brushes: Influence of polymer chain length and temperature.
683 Langmuir **2004**, 20, 10949−10955.
684 [56] Mi, B.; Elimelech, M. Chemical and physical aspects of organic fouling of forward
685 osmosis membranes. J. Membr. Sci. **2008**, 320,292−302.
686 [57] Li, Q.; Elimelech, M. Organic fouling and chemical cleaning of nanofiltration
687 membranes: Measurements and mechanisms. Environ. Sci. Technol. **2004**, 38,
688 4683−4693.